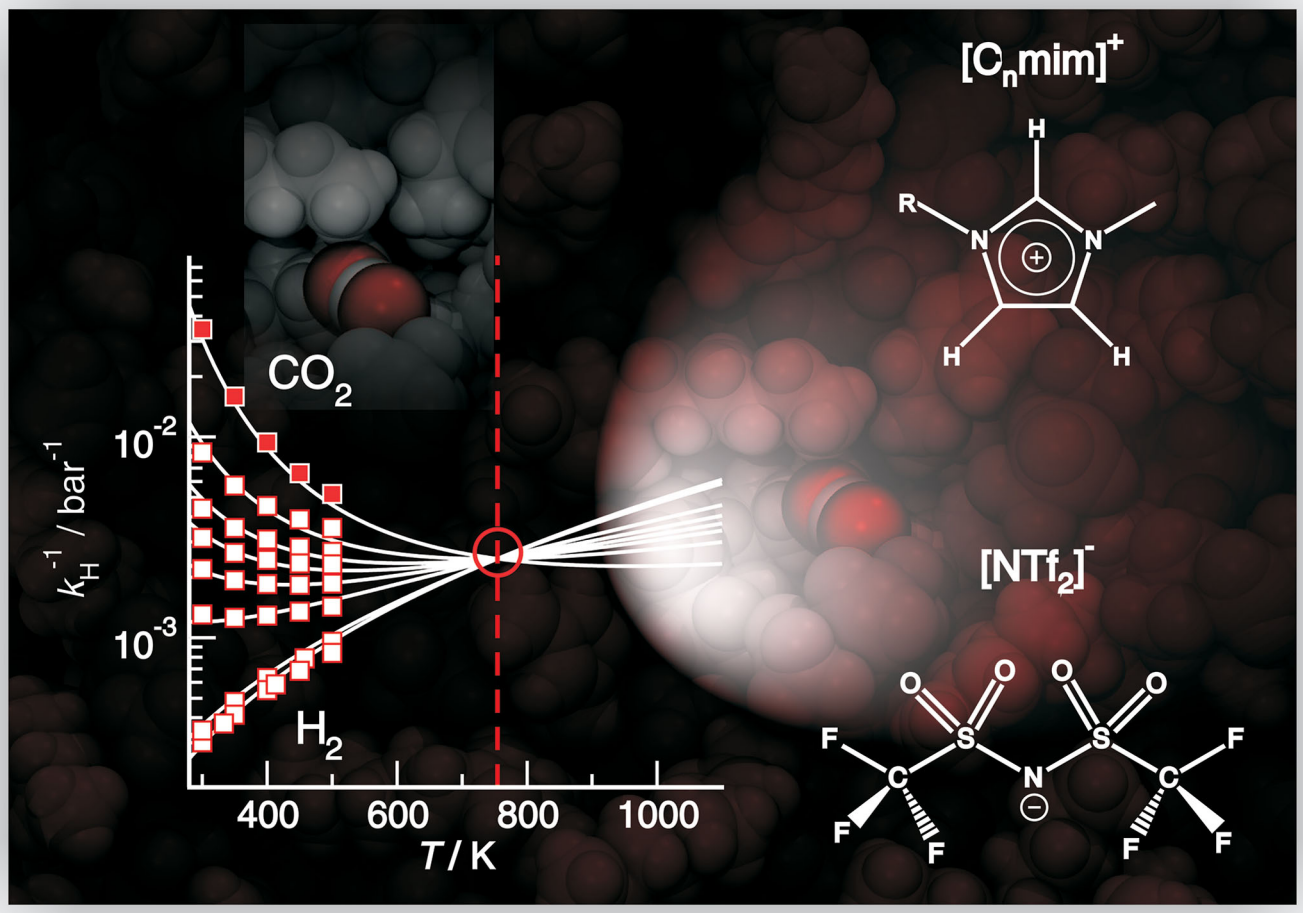

Showcasing work by Daniela Kerlé, Majid Namayandeh Jorabchi, Ralf Ludwig, Sebastian Wohlrab und Dietmar Paschek from Physical and Theoretical Chemistry at the University of Rostock, Germany.

A simple guiding principle for the temperature dependence of the solubility of light gases in imidazolium-based ionic liquids derived from molecular simulations

This article reports the temperature dependence of the solvation behaviour of light gases in ionic liquids. Extensive molecular dynamics simulations show that the solubility of gases ranging from molecular hydrogen to carbon dioxide is determined by entropy–enthalpy compensation. Our model can provide reliable estimates for the solvation behaviour, where conflicting or no experimental data exist.

As featured in:

See Daniela Kerlé, Ralf Ludwig, Dietmar Paschek *et al.*, *Phys. Chem. Chem. Phys.*, 2017, **19**, 1770.

ROYAL SOCIETY OF CHEMISTRY

rsc.li/pccp

Registered charity number: 207890

PCCP

PAPER

View Article Online
View Journal | View Issue

Cite this: *Phys. Chem. Chem. Phys.*, 2017, **19**, 1770

A simple guiding principle for the temperature dependence of the solubility of light gases in imidazolium-based ionic liquids derived from molecular simulations

Daniela Kerlé,*[a] Majid Namayandeh Jorabchi,[b] Ralf Ludwig,*[bc] Sebastian Wohlrab[c] and Dietmar Paschek*[b]

Received 4th October 2016,
Accepted 8th November 2016

DOI: 10.1039/c6cp06792a

www.rsc.org/pccp

We have determined the temperature dependence of the solvation behavior of a large collection of important light gases in imidazolium-based ionic liquids with the help of extensive molecular dynamics simulations. The motivation of our study is to unravel common features of the temperature dependent solvation under well controlled conditions, and to provide a guidance for cases, where experimental data from different sources disagree significantly. The solubility of molecular hydrogen, oxygen, nitrogen, methane, krypton, argon, neon and carbon dioxide in the imidazolium based ionic liquids of type 1-*n*-alkyl-3-methylimidazolium bis(trifluoromethylsulfonyl)imide ([$C_n$mim][NTf_2]) with varying alkyl side chain lengths n = 2, 4, 6, 8 is computed for a temperature range between 300 K and 500 K at 1 bar. By applying Widom's particle insertion technique and Bennet's overlapping distribution method, we are able to determine the temperature dependent solvation free energies of those selected light gases in simulated imidazolium based ionic liquids with high statistical accuracy. Our simulations demonstrate that the magnitude of the solvation free energy of a gas molecule at a chosen reference temperature and that of its temperature-derivatives are intimately related to one another. We conclude that this "universal" behavior is rooted in a solvation entropy–enthalpy compensation effect, which seems to be a defining feature of the solvation of small molecules in ionic liquids. The observations lead to simple analytical relations, determining the temperature dependence of the solubility data based on the absolute solubility at a certain reference temperature. By comparing our results with available experimental data from many sources, we can show that our approach is particularly helpful for providing reliable estimates for the solvation behavior of very light gases, such as hydrogen, where conflicting experimental data exist.

1 Introduction

Salts with melting points below 100 °C are commonly referred to as ionic liquids (ILs). These liquids have several unique properties,[1–4] and are used for a wide range of potential applications.[5,6] For the application of ILs in gas separation processes (*e.g.* flue gas decontamination) it is important to have access to accurate solubility data.[7–10] Even more so, the recently introduced supported ionic liquid membranes[11–14] are promising new tools for separating various mixtures of gases. Of particular importance, of course, is the ability to separate H_2 and CO_2 from gas-streams.

Till now, a wealth of experimental measurements of the infinite dilution properties of a large number of gases in various ILs have been reported.[15] However, the experimental determination of solubilities is particularly difficult for gases with a low molecular weight.[1] As a result, the reported solubility data of hydrogen in ILs[16–26] are highly inconsistent.

In addition, theoretical methods to determine solubilities of gases in imidazolium-based ILs have been reported in the literature: data were determined from COSMO based methods,[27–30] equations of state approaches,[31–34] group theory,[35] quantitative structure–property relationship (QSPR) and neutral network models,[36] as well as molecular dynamics (MD) and Monte Carlo (MC) simulations.[37–54] We would like to point out that MD and MC simulations have the advantage that they offer the possibility of both a (semi-)quantitative prediction of the solubility and gaining a fundamental understanding of the molecular mechanism for the solvation process.

For the simulation of imidazolium-based ILs there are different atomic-detailed molecular force fields available.[55]

[a] *Universität Bremen, Fachbereich Produktionstechnik, Technische Thermodynamik, Badgasteiner Str. 1, D-28359 Bremen, Germany. E-mail: dkerle@uni-bremen.de; Fax: +49 421 218 64771; Tel: +49 421 218 64757*
[b] *Universität Rostock, Institut für Chemie, Physikalische und Theoretische Chemie, Dr.-Lorenz-Weg 1, D-18059 Rostock, Germany*
[c] *Leibniz-Institut für Katalyse an der Universität Rostock, Albert-Einstein-Str. 29a, D-18059 Rostock, Germany*

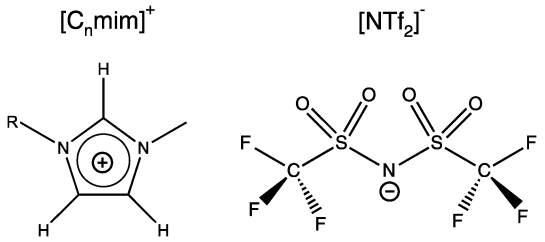

Fig. 1 Schematic representation of the studied ionic liquids 1-*n*-alkyl-3-methylimidazolium bis(trifluoromethylsulfonyl)imide [C$_n$mim][NTf$_2$].

Many of those force-fields are capable of reproducing essentially "static" properties, such as thermodynamic properties and structural features quite well. However, most of them are lacking the ability of describing transport properties, such as diffusion coefficients and viscosities satisfactorily. In this study we used the non-polarizable all-atom force field originally introduced by Lopes,[56] using the refined parameters from the study by Köddermann *et al.*[57] to simulate the imidazolium-based ILs of type [C$_n$mim][NTf$_2$] (see Fig. 1). We have shown earlier that a wealth of both thermodynamical and dynamical properties of the pure IL could be described in excellent agreement with experimental data[40,57] by using this model. In addition, this modified force field was also capable of describing the solvation behavior of noble gases[58] and carbon dioxide[59] very satisfactorily. By accurately determining temperature dependent solvation properties, we could demonstrate that the entropy contribution to the solvation free energy plays an important role in the solvation process, not unlike the hydrophobic hydration of small apolar particles in liquid water.[60–63] Moreover, also an entropy-driven "solvophobic interaction" of apolar particles could be observed in ILs,[58] indicating that specific solvent-mediated interactions could play an important role in ILs.

Here we focus on the infinite dilution properties of "light gases", like carbon dioxide, oxygen, nitrogen, methane, argon, neon, and hydrogen in imidazolium based ILs. The chosen gases cover a spectrum from very weakly interacting gases, such as hydrogen, to moderately strong interacting molecules, such as carbon dioxide. We apply Widom's particle insertion technique for calculating temperature dependent solvation free energies and solubilities of these gases in imidazolium-based ILs of the type [C$_n$mim][NTf$_2$] with varying chain lengths n = 2, 4, 6, 8. In addition, to validate these calculations we also use Bennett's overlapping distribution method for selected examples. Calculated Henry's law constants are compared with available experimental data. The temperature behavior of the solubility as well as its dependence of the alkyl chain lengths in the imidazolium cations is determined and discussed. The motivation of our study is to reveal common "universal" features of the temperature dependent solvation under well controlled conditions, and to provide a reasonable guidance for cases, where experimental data from different sources disagree significantly.

2 Experimental section

2.1 Molecular dynamics simulations

We perform constant pressure (*NPT*) MD simulations of imidazolium based ILs of the type [C$_n$mim][NTf$_2$] for different chain lengths n = 2, 4, 6, 8 at a pressure of 1 bar, covering a broad temperature range between 300 K and 500 K. All simulated systems are composed of 343 ion pairs, applying the force field from the study by Köddermann *et al.*[57] An additional minor modification from the simulation setup used in previous studies[40,57] is that all bond-lengths were kept fixed. As shown before[59] this does not have any impact on the studied properties. A cubic simulation box was used, and the system size with 343 ion pairs was chosen, which is large enough that thermodynamical properties do not depend on the system size, as it was reported by Wittich *et al.*[64] for a system of 125 ion pairs of [C$_4$mim][PF$_6$]. For the solutes, various models from the literature without modification of the interacting parameters were employed. For hydrogen, the potential obtained from the study by Potkowski *et al.*[65] was used. Potential modes reported by Guillot *et al.*[66] were employed to describe the noble gases and methane. Nitrogen was described by the potential obtained from the study by Potoff *et al.*[67] and oxygen by the potential obtained from the study by Hansen *et al.*[68] Finally, carbon dioxide the EPM2-model of Harris and Yung[69] was used in a modified way as described before.[59] All parameters describing the solutes are given in Table 1.

All simulations reported here were performed using the Gromacs simulation program.[70] The preparation of topology files, as well as the data analysis, was performed using the most recent version of the MOSCITO suite of programs.[71] Production runs of 10 ns length were employed for every temperature, starting from previously well equilibrated configurations. To avoid artifacts due to slow dynamics at low temperatures these systems were pre-equilibrated at 500 K. A Nosé–Hoover thermostat[72,73] and a Parrinello–Rahman barostat[74,75] with coupling times τ_T = 1.0 ps and τ_p = 2.0 ps were used to control constant temperature and pressure (1 bar) conditions. The electrostatic interactions were treated by particle mesh Ewald summation.[76] A real space cutoff of 1.2 nm was employed, and a mesh spacing of approximately 0.12 nm (4th order interpolation) had been used to determine the reciprocal lattice contribution. The Ewald convergence parameter was set to a relative accuracy of the Ewald sum of 10^{-5}. Lennard-Jones cutoff corrections for energy and pressure were considered.

Table 1 Force field parameters describing the studied gaseous solutes. Given are the Lennard-Jones parameter for the solute–solute site–site interactions σ_{ii}, and ε_{ii}, the partial charges q_i, as well as the intramolecular bond-lengths d. Lennard-Jones cross parameters for the solute–solvent interactions were obtained from Lorentz–Berthelot combination rules

		$\varepsilon_{ii}\cdot k_B^{-1}$/K	σ_{ii}/Å	$q_i/\lvert e\rvert$	d/Å
H_2[65]		35.45	3.46		
Ne[66]		18.6	3.035		
Ar[66]		125.0	3.415		
Kr[66]		169.0	3.675		
CH_4[66]		147.4	3.73		
N_2[67]	N	36.0	3.31	−0.482	1.10
	COM			+0.964	
O_2[68]	O	49.048	3.013	−0.123	1.21
	COM			+0.246	
CO_2[69]	C	28.129	2.757	+0.6512	1.149
	O	80.507	3.033	−0.3256	

A 2 fs timestep was used in all simulations, and in every 25th step a configuration was saved. Distance constraints were solved by means of the SHAKE procedure.[77] The thermodynamic properties of the simulated ILs are essentially identical to the properties reported in ref. 59.

2.2 Infinite dilution properties

The solubility of a solute A in a solvent B is conveniently described by the Ostwald coefficient $L^{l/g} = \rho_A^l/\rho_A^g$, where ρ_A^l and ρ_A^g are the number densities of the solute in the liquid and the gas phase of component B, respectively, when both phases are in equilibrium. Alternatively, the solubility of solute A can be expressed in terms of the inverse Henry's law constant k_H^{-1}. The relationship between Henry's law constant and the excess chemical potential $\mu_{ex,A}^l$ in the liquid phase is given by[78]

$$k_H^{-1} = \exp[-\beta\mu_{ex,A}^l]/(\rho_{IL}^l RT), \quad (1)$$

where $\beta = 1/k_B T$ and ρ_{IL}^l represents the number-density of ion pairs in the IL solvent.

According to Widom's potential distribution theorem,[79,80] the excess chemical potential μ_{ex} can be computed as a volume weighted ensemble average

$$\mu_{ex} = -k_B T \ln\langle V \exp(-\beta\Phi)\rangle/\langle V\rangle. \quad (2)$$

Here V is the volume of the simulation box and Φ is the energy of a gas molecule inserted at a random position with a random orientation. The brackets $\langle\cdots\rangle$ indicate isothermal–isobaric averaging over many configurations, as well as averaging over many insertions.

As control, we also determine the excess chemical potential from energy histograms[81,82] computed for the energy change $\Delta U = U(N+1) - U(N)$ associated with the insertion $p_0(\Delta U)$ and removal $p_1(\Delta U)$ of an $(N+1)$th gas molecule from the constant pressure (NPT) simulation. The two distribution functions are related according to

$$p_1(\Delta U) = \frac{Q(N,P,T)}{Q(N+1,P,T)}\frac{\langle V\rangle}{\Lambda^3} \times \exp(-\beta\Delta U)p_0(\Delta U), \quad (3)$$

using the definition of the ideal and excess part of the chemical potential μ referring to the ideal gas state with the same average number-density,[83] a relation between the two distribution functions and the excess chemical potential is obtained, which is analogous to the expression for the canonical ensemble[83]

$$\ln p_1(\Delta U) - \ln p_0(\Delta U) = \beta\mu_{ex} - \beta\Delta U. \quad (4)$$

The only difference is the necessity of volume-weighting in the calculation of the $p_0(\Delta U)$-distribution function.[84] For reasons of convenience we define functions f_0 and f_1 according to

$$f_0(\Delta U) = \beta^{-1}\ln p_0(\Delta U) - \frac{\Delta U}{2},$$

and

$$f_1(\Delta U) = \beta^{-1}\ln p_1(\Delta U) + \frac{\Delta U}{2},$$

such that

$$\mu_{ex} = f_1(\Delta U) - f_0(\Delta U). \quad (5)$$

All computed energies are based on the minimum image and include a reaction field correction similar to Roberts and Schnitker.[85] Cut-off corrections for the dispersion interactions are included.[86] A total of 2×10^5 configurations were analyzed for each IL and for every temperature. Each configuration was sampled by 10^3 random insertions to determine the f_0-functions. The energies computed for those insertions have also been used to determine "Widom-estimates" for the excess chemical potentials. We would like to point out that the values computed from particle insertions are found to lie within the statistical uncertainty of the data from the overlapping distribution theory. Note that the choice of the sampling rate is a critical parameter for successfully computing the chemical potentials *via* Widom's insertion technique. By reducing the sampling rate significantly, we denote a systematic deviation of the "Widom-estimate" from the data obtained *via* the overlapping distribution method. This effect was observed by us for sampling rates being about two orders of magnitude lower than the rates reported here. All "converged" computed Henry coefficients are shown in Table 2.

From the temperature dependence of the computed solvation free energy for infinite dilution, we can comment on the behavior of the first and second derivatives of free energy with respect to temperature. So the solvation entropies, enthalpies, and heat capacities are obtained from fits of the data to a second order expansion of the solvation free energy around the reference state (T° = 298 K at P° = 1 bar) according to

$$\mu_{ex}(T) = \mu_{ex}^\circ - s_{ex}^\circ(T - T^\circ) - c_{P,ex}\left[T\left(\ln T/T^\circ - 1\right) + T^\circ\right]. \quad (6)$$

Here μ_{ex}° and s_{ex}° represent the solvation free energy and the solvation entropy in the reference state, respectively, relating the corresponding enthalpy h_{ex}° and entropy s_{ex}° *via* $h_{ex}^\circ = \mu_{ex}^\circ + T^\circ s_{ex}^\circ$. According to the second order expansion, the solvation heat capacity $c_{P,ex}$ is assumed to be constant over the considered temperature range. The fitted parameters are provided in Table 3.

3 Results and discussion

We have computed the solvation free energies μ_{ex} and the associated Henry coefficients k_H of CO_2, O_2, N_2, CH_4, Kr, Ar, Ne and H_2 at infinite dilution from MD simulations for the four ILs $[C_n\text{mim}][NTf_2]$ with n = 2, 4, 6, 8, employing the sampling techniques discussed in the previous section. The density data for the simulated IL necessary to inter-convert Henry coefficients k_H and solvation free energies μ_{ex} can be found in ref. 59. All computed Henry coefficients are summarized in Table 2. The temperature dependence of the corresponding solvation free energies $\mu_{ex}(T)$ has been fitted to a second order expansion around a reference state following eqn (6). The parameters obtained for a reference temperature of T° = 298 K are given in Table 3. In Fig. 2 computed solubilities (here given as inverse Henry's law constants) are compared with available experimental and theoretical data. For reasons of clarity, we restrict this comparison to data based on solvation in $[C_6\text{mim}][NTf_2]$,

Table 2 Calculated Henry coefficients k_H for various gaseous components dissolved in imidazolium based ILs of type $[C_n\text{mim}][NTf_2]$. All data were obtained from MD simulations at 1 bar and describe the infinite dilution limit according to $k_H = \exp[\beta\mu^{\infty}_{ex,gas}] \times \rho^{\infty}_{IL}RT$.[78] The ion pair densities are computed from fitted second order polynomial ρ^{∞}_{IL}[87]

		k_H/bar			
	T/K	[C_2mim]	[C_4mim]	[C_6mim]	[C_8mim]
CO_2	300	34 ± 3	28 ± 3	29 ± 3	22 ± 3
	350	87 ± 6	73 ± 5	63 ± 4	56 ± 6
	400	140 ± 8	121 ± 6	107 ± 6	98 ± 9
	450	207 ± 10	171 ± 9	152 ± 8	139 ± 11
	500	262 ± 12	224 ± 11	191 ± 9	185 ± 13
Kr	300	188 ± 5	143 ± 6	119 ± 6	89 ± 6
	350	266 ± 4	210 ± 3	175 ± 2	139 ± 3
	400	327 ± 3	261 ± 3	221 ± 2	182 ± 3
	450	377 ± 2	306 ± 2	257 ± 1	214 ± 1
	500	411 ± 2	337 ± 3	284 ± 2	240 ± 1
CH_4	300	300 ± 10	224 ± 15	214 ± 15	142 ± 10
	350	381 ± 7	300 ± 7	277 ± 6	203 ± 5
	400	441 ± 3	351 ± 4	321 ± 4	249 ± 3
	450	486 ± 5	391 ± 3	353 ± 3	278 ± 2
	500	509 ± 4	415 ± 3	373 ± 3	299 ± 2
Ar	300	436 ± 9	350 ± 12	318 ± 14	242 ± 15
	350	508 ± 6	418 ± 6	378 ± 4	303 ± 6
	400	548 ± 4	455 ± 5	410 ± 4	340 ± 4
	450	571 ± 3	478 ± 3	427 ± 2	356 ± 2
	500	577 ± 2	486 ± 3	431 ± 3	365 ± 2
O_2	300	652 ± 22	523 ± 21	456 ± 23	378 ± 26
	350	720 ± 7	596 ± 8	517 ± 5	447 ± 10
	400	744 ± 5	619 ± 7	540 ± 5	480 ± 6
	450	750 ± 5	629 ± 4	545 ± 3	482 ± 3
	500	732 ± 4	621 ± 5	536 ± 3	477 ± 3
N_2	300	1048 ± 47	858 ± 42	766 ± 46	651 ± 53
	350	1062 ± 15	898 ± 14	795 ± 12	707 ± 20
	400	1036 ± 7	875 ± 11	775 ± 9	703 ± 11
	450	991 ± 8	844 ± 7	741 ± 4	666 ± 6
	500	942 ± 4	802 ± 7	699 ± 4	629 ± 5
Ne	300	3418 ± 63	3051 ± 88	2898 ± 110	2752 ± 172
	350	2507 ± 23	2222 ± 25	2088 ± 16	1964 ± 36
	400	1943 ± 13	1716 ± 10	1587 ± 13	1480 ± 8
	450	1570 ± 12	1388 ± 8	1267 ± 5	1185 ± 10
	500	1318 ± 6	1147 ± 5	1047 ± 5	977 ± 7
H_2	300	3875 ± 98	3286 ± 121	3313 ± 157	2718 ± 173
	350	2867 ± 42	2466 ± 44	2415 ± 33	2066 ± 42
	400	2216 ± 16	1906 ± 23	1835 ± 19	1610 ± 21
	450	1805 ± 22	1552 ± 10	1462 ± 7	1279 ± 9
	500	1510 ± 5	1296 ± 10	1190 ± 13	1058 ± 8

Table 3 Thermodynamic parameters describing the temperature dependence of the solvation free energies $\mu_{ex}(T)$ of the indicated solutes according to a second order expansion around a thermodynamic reference state, following eqn (6). The chosen reference state has been set to T° = 298 K at P° = 1 bar

		[C_2mim]	[C_4mim]	[C_6mim]	[C_8mim]
CO_2	μ°_{ex}/kJ mol^{-1}	−2.57	−2.79	−2.45	−2.89
	s°_{ex}/J K^{-1} mol^{-1}	−39.1	−40.1	−33.8	−39.2
	h°_{ex}/kJ mol^{-1}	−14.2	−14.7	−12.5	−14.6
	$c_{P,ex}$/J K^{-1} mol^{-1}	45	48	34	43
Kr	μ°_{ex}/kJ mol^{-1}	1.66	1.24	1.09	0.56
	s°_{ex}/J K^{-1} mol^{-1}	−20.5	−21.3	−20.9	−23.1
	h°_{ex}/kJ mol^{-1}	−4.45	−5.09	−5.13	−6.32
	$c_{P,ex}$/J K^{-1} mol^{-1}	19.9	21.9	21.7	26.8
CH_4	μ°_{ex}/kJ mol^{-1}	2.78	2.36	2.55	1.73
	s°_{ex}/J K^{-1} mol^{-1}	−18.5	−19.7	−18.4	−21.8
	h°_{ex}/kJ mol^{-1}	−2.72	−3.50	−2.92	−4.76
	$c_{P,ex}$/J K^{-1} mol^{-1}	17.6	20.8	18.6	27.0
Ar	μ°_{ex}/kJ mol^{-1}	3.76	3.48	3.54	3.06
	s°_{ex}/J K^{-1} mol^{-1}	−16.2	−16.7	−16.6	−18.4
	h°_{ex}/kJ mol^{-1}	−1.07	−1.51	−1.42	−2.41
	$c_{P,ex}$/J K^{-1} mol^{-1}	16.9	18.4	19.3	23.5
O_2	μ°_{ex}/kJ mol^{-1}	4.76	4.48	4.43	4.17
	s°_{ex}/J K^{-1} mol^{-1}	−16.8	−17.2	−17.1	−19.0
	h°_{ex}/kJ mol^{-1}	−0.23	−0.66	−0.67	−1.50
	$c_{P,ex}$/J K^{-1} mol^{-1}	19.0	20.0	20.7	26.0
N_2	μ°_{ex}/kJ mol^{-1}	5.95	5.72	5.73	5.53
	s°_{ex}/J K^{-1} mol^{-1}	−15.5	−16.4	−16.2	−18.4
	h°_{ex}/kJ mol^{-1}	1.34	0.84	0.90	0.04
	$c_{P,ex}$/J K^{-1} mol^{-1}	17.0	20.0	21.0	27.6
Ne	μ°_{ex}/kJ mol^{-1}	8.89	8.90	9.07	9.13
	s°_{ex}/J K^{-1} mol^{-1}	−5.66	−5.91	−5.36	−4.96
	h°_{ex}/kJ mol^{-1}	7.20	7.14	7.47	7.65
	$c_{P,ex}$/J K^{-1} mol^{-1}	10.1	12.3	11.7	10.8
H_2	μ°_{ex}/kJ mol^{-1}	9.19	9.09	9.40	9.11
	s°_{ex}/J K^{-1} mol^{-1}	−7.29	−7.72	−7.29	−8.99
	h°_{ex}/kJ mol^{-1}	7.02	6.79	7.23	6.43
	$c_{P,ex}$/J K^{-1} mol^{-1}	11.3	13.4	14.9	19.0

because most experimental datasets are only available for this particular IL, since it had been selected as a reference compound for an IUPAC experimental validation project.[88,89]

The remainder of this section is organized as follows: first we will compare our simulated solubility data with available experimental and theoretical data. A short discussion of the available solubility data is given for every gas in detail. The following sections will then focus on a systematic rationalization of the effect of varying the alkyl side chain length, and of changing the temperature based on an enthalpy–entropy compensation behavior obeyed by all the considered gases.

3.1 Comparison with available experimental and theoretical data

Carbon dioxide. For carbon dioxide we have shown previously[59] that all available experimental and theoretical data are in excellent agreement with our simulation results. In particular, the temperature dependence is reflected very well by the simulations.[16,18,90,91] Moreover, we could recently show that small differences with respect to a few experimental datasets could be explained by water content in the samples.[92]

Methane. Experimental data for the solubility of methane are available from various sources. Kumełan *et al.*[49] examined methane in $[C_6\text{mim}][NTf_2]$ over a large temperature range. In addition, the data obtained from the study by Finotello *et al.*[16]

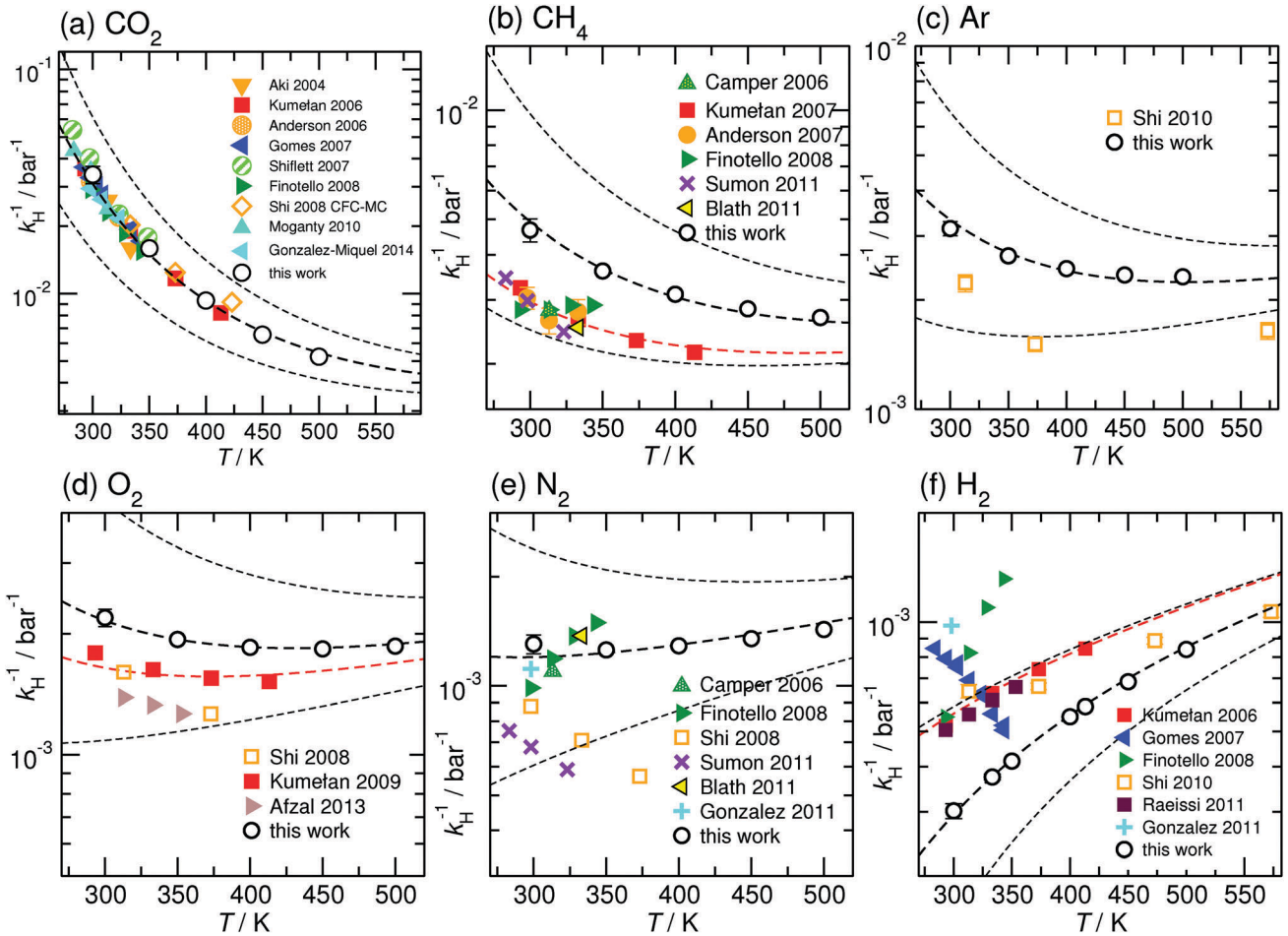

Fig. 2 Solubilities $k_H^{-1} = \exp[-\beta\mu^{\infty}_{ex,gas}]/\rho^{\infty}_{IL}RT$ of selected gases in [C_6mim][NTf_2]. Shown are data for (a) CO_2, (b) CH_4, (c) Ar, (d) O_2, (e) N_2, and (f) H_2 at 1 bar. The filled symbols represent experimental data given according to the indicated sources. Open symbols specify data from molecular simulations, while crosses represent data obtained from alternative theoretical predictions. All dashed lines show theoretical predictions based on our enthalpy–entropy compensation model. The upper and lower black thin dashed lines are temperature-predictions for solubilities twice and half of the reference-value used for our MD simulation-data (given as black thick dashed lines). The red dashed line represents an enthalpy–entropy compensation model prediction for the experimental solubility data obtained from the study by Kumełan *et al.* References for the experimental and theoretical data are given in the text. Error bars are shown where they were available and are not smaller than the symbol size.

are shown, who investigated [C_2mim][NTf_2] and [C_6mim][NTf_2]. Moreover, we also show the data according to Camper *et al.*,[93] as well as Anderson *et al.*,[94] and Blath *et al.*[95] for [C_6mim][NTf_2]. Our data predict a systematically higher solubility compared with the mostly consistent experimental datasets, but are in good agreement with the temperature slope of the data obtained from the study by Kumełan *et al.* The temperature dependencies reported by Finotello and Anderson, however, are clearly not compatible with our findings and the data obtained from the study by Kumełan *et al.* We would like to point out that we did not perform any adjustment to the force field parameters to improve the solute–solvent interaction. The Lennard-Jones parameters used by us from the study by Guillot *et al.*[66] apparently overestimate the interaction between the solvent and the solute. The data calculated for CH_4 by Sumon *et al.* using COSMO-RS[30] show the same temperature trend for methane as our simulations.

Noble gases. For the case of krypton there is only one experimental dataset available, published by Afzal *et al.*[96] in 2013 (not shown here). It shows the same temperature trend as our simulated results. For the case of argon and neon, to our knowledge, no experimental data are available. In 2010 Shi *et al.*[52] published Henry's law constants obtained from computer simulations of argon in [C_6mim][NTf_2]. Their data are in the same decade compared to ours, and the temperature dependence is similar, but their computed solubilities are slightly smaller.

Oxygen. For the case of oxygen, there are only a few experimental solubility datasets available. This is likely due to the experimental challenges associated with the use of oxygen. Our data apparently slightly overestimate the solubility of oxygen, but seem to agree particularly well with the slope of the temperature dependence reported by Kumełan *et al.*[97] in [C_6mim][NTf_2]. The temperature dependent data obtained from the study by Anthony *et al.*[98] for [C_4mim][NTf_2] (not shown here), however, suggest a significantly stronger temperature dependence, in accordance with the recently published values in the study by Afzal *et al.*[96] The simulation-based data obtained from the study

by Shi *et al.*[38] seem to be placed right in the middle between the data obtained from the study by Afzal *et al.* and Kumełan *et al.*

Nitrogen. The solubility of nitrogen has been studied by several groups. Unfortunately, the temperature trends of the available experimental and theoretical datasets seem to be quite inconsistent. The data obtained from the study by Camper *et al.*[93] and Finotello *et al.*[16] in [C_2mim][NTf_2] and [C_6mim][NTf_2], as well as Blath *et al.*[95] (measured at 60 °C in [C_6mim][NTf_2]), are very close with respect to each other. Our data is in the same range as the experimental data, however, we do not observe a significant increase of the computed solubilities with increasing temperature. Both the data calculated for N_2 by Sumon *et al.*[30] using COSMO-RS[30] and Shi *et al.*[38] using computer simulation techniques show a significantly different temperature dependence compared to the experimental datasets obtained from the study by Finotello *et al.*

Hydrogen. For the solubility of molecular hydrogen, experimental data from various groups are available. However, different groups report substantially different, inconsistent results. Dyson *et al.*[20] just published one value for [C_4mim][NTf_2]. The group of Costa Gomes[17,18] has studied [C_2mim][NTf_2], [C_4mim][NTf_2] and [C_6mim][NTf_2] and found decreasing solubility with increasing temperature. In stark contrast to the findings of Costa Gomes, Finotello *et al.*,[16] who examined [C_2mim][NTf_2] and [C_6mim][NTf_2], found a strongly increasing solubility with increasing temperature. Kumełan *et al.*[99] observed this trend as well for [C_6mim][NTf_2], albeit with a significantly weaker temperature dependence. The experimental data obtained from the study by Raeissi *et al.*[26] seem to match almost exactly the data obtained from the study by Kumełan *et al.* using a similar experimental set-up. Shi *et al.*[52] published Henry's law constants for hydrogen in [C_6mim][NTf_2] from computer simulations. Their results support our result of a positive slope of the temperature dependent solubility data and match very well the values of Kumełan *et al.* as well as Raeissi *et al.*

3.2 Alkyl side chain length dependence

The computed solubilities as a function of the alkyl side chain length obtained from MD simulation are given as inverse Henry coefficients, and are shown as full symbols in Fig. 3. The data indicate a rather small variation of Henry coefficients for ILs with varying chain lengths. However, there is a tendency towards higher solubilities for gases in ILs with longer alkyl side chains. When comparing the solubility data for [C_2mim][NTf_2] and [C_8mim][NTf_2] for all the investigated gases, we consistently observe an increase in solubility of about 30% to 40% for the component with the C8-chain. In ref. 59 we reported the observation that the solvation free energies μ_{ex} of carbon dioxide showed almost no chain length dependence at a given temperature. By assuming μ_{ex} to be chain length independent, it follows that the chain length dependence of the solubility data at a given temperature can be solely expressed due to density scaling according to eqn (1), leading to an approximate expression:

$$k_H^{-1}(\rho_{IL}') \approx k_H^{-1}(\rho_{IL}) \times \frac{\rho_{IL}}{\rho_{IL}'}, \quad (7)$$

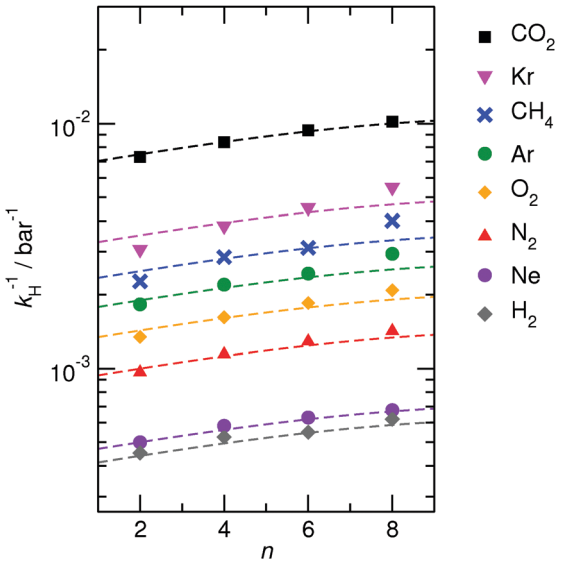

Fig. 3 Comparison of inverse Henry coefficients of all simulated gases in [$C_n$mim][NTf_2] with varying chain lengths n = 2, 4, 6, 8 at 400 K. The dashed lines are predictions of the chain length dependence based on the density scaling procedure described in eqn (7).

where ρ_{IL} and ρ_{IL}' represent the number-densities of the ion pairs in ILs with different alkyl side chain lengths. Using the density data of our simulated ILs (data are given in ref. 59), we have fitted the number-density as a function of chain length n to a second order polynomial:

$$\rho_{IL}(n) = \rho_{IL}^{(0)} + \rho_{IL}^{(1)} \cdot n + \rho_{IL}^{(2)} \cdot n^2 \quad (8)$$

with $\rho_{IL}^{(0)}$ = 2.406 nm^{-3}, $\rho_{IL}^{(1)}$ = −0.1584 nm^{-3}, and $\rho_{IL}^{(2)}$ = 6.39 × 10^{-3} nm^{-3} for T = 400 K. As shown in Fig. 3, the rather simple density scaling procedure describes rather accurately the chain length dependence of the solubility data of the entire set of gases, suggesting that the condition $\mu_{ex}(n) \approx$ const. is mostly fulfilled for those gases.

3.3 Temperature dependence: enthalpy–entropy compensation effect

From the wealth of experimental and theoretical solubility data presented in Fig. 2 (including our data) we conclude that there apparently exists a systematic relationship between the temperature dependent slope of the solubilities of different gases and their interaction-strength with the solvent: rather "strongly" interacting species, such as CO_2, show apparently a strong "anomalous" temperature dependence of the solubility, whereas weakly interacting species such as oxygen and argon show a significantly weaker temperature behavior. Finally, for the case of molecular hydrogen (H_2), we observe a change in the sign of the slope, showing a strongly increasing solubility with increasing temperature. The latter finding is apparently supported by the majority of experimental datasets. However, for two cases, namely nitrogen and hydrogen, there are substantially conflicting results from different sources, each suggesting a very different kind of temperature behavior. How could this be resolved? We think that the apparent systematic trend is deeply

rooted in the free energy landscape explored by a solvated gas molecule, and that the observed trend can be explained by purely thermodynamic means.

By fitting the temperature dependent solvation free energies $\mu_{ex}(T)$ to the second order expansion around a thermodynamic reference state (T° = 298 K and P° = 1 bar) given by eqn (6), we obtain standard solvation free energies μ°_{ex}, entropies s°_{ex}, enthalpies h°_{ex}, as well as the solvation heat capacities $c^\circ_{P,ex}$. Data computed for all studied gases and ILs are collected in Table 3. In addition, we also consider data for a modified CO_2 molecule, where we have systematically weakened the interaction with the solvent by switching off the Coulomb interaction, and by scaling the Lennard-Jones interaction using a factor f with $\varepsilon_{ij} = (f\varepsilon_{ii}\varepsilon_{jj})^{1/2}$. Finally, this prototypical molecule is transformed into a purely repulsive component by modeling the solute–solvent interaction solely *via* Weeks–Chandler–Andersen-type (WCA) interactions according to $V_{ij}(r) = V_{ij,LJ}(r) + \varepsilon_{ij}$ for $r \leq r_{LJ,min}$, and $V_{ij}(r) = 0$ otherwise. Following the procedure suggested by Simha *et al.* for the dissolution of gases in polymers,[100,101] Fig. 4a shows a plot of the standard solvation free energy μ°_{ex} *vs.* the solvation enthalpy h°_{ex} for all studied gases in all solvents. It is evident that both properties are linearly related for the entire set of solvation data. This linear relationship can be utilized to predict the temperature dependent solvation data. Furthermore, it can provide us with a quantitative representation of the notion that the absolute solubility of a certain compound and its temperature behavior are somehow related. The thermodynamic definition of the free energy implies that the solvation entropy and enthalpy have to be linearly related as well, as it is demonstrated in Fig. 4b. To quantify the relations shown in Fig. 4 we use the following relation:

$$h^\circ_{ex} = a \cdot \mu^\circ_{ex} + b, \tag{9}$$

with a = 1.653 and b = −7.87 kJ mol^{-1}, representing the parameters used for plotting the dashed lines shown in Fig. 4a and b.

From eqn (9) the relation between s°_{ex} and h°_{ex} can be obtained as

$$T^\circ s_{ex} = h^\circ_{ex} \cdot \frac{a-1}{a} + \frac{b}{a}. \tag{10}$$

The excellent correlation between s°_{ex} and h°_{ex} over a rather wide range of interaction strengths is apparently intimately related to the process of solvation of small gas molecules. In particular, how a gas molecule and its solvation shell explore the configurational space of the solvated state. The consequence is a positive correlation between the solvation entropy and the solvation enthalpy. We would like to point out that by restricting our study to "small gas molecules", the variation in the size of the molecules has apparently no big effect, and is being accounted for effectively. For larger solutes this might not necessarily be the case.

The relationship between s°_{ex} and μ°_{ex} as outlined above essentially determines the coupling between the absolute solubility and its temperature dependence. However, the second order expansion of $\mu_{ex}(T)$ given in eqn (6) also requires the knowledge of the heat capacity of solvation $c_{P,ex}$, to fully determine the temperature dependence of all our solubility data. Fortunately, the variation of the computed $c_{P,ex}$-values, given in Table 3, and shown in Fig. 5, has no big effect. If we neglect the heat capacity contribution completely by setting $c_{P,ex}$ = 0, we arrive at a description, which is qualitatively correct for all investigated gases (not shown). This procedure, however, leads to significant deviations of the predicted data from our simulation data for temperatures above 400 K. A much better description is achieved by using a common value of $c_{P,ex}$ = 20 J K^{-1} mol^{-1} for all gases instead, as it is indicated by the predictions represented by thin dashed lines in Fig. 6. However, to improve things further, we make use of a negative correlation between μ°_{ex} and $c_{P,ex}$, suggested in Fig. 5. To complete our model we make use of the linear relationship between μ°_{ex} and $c_{P,ex}$:

$$c_{P,ex} = c \cdot \mu^\circ_{ex} + d \tag{11}$$

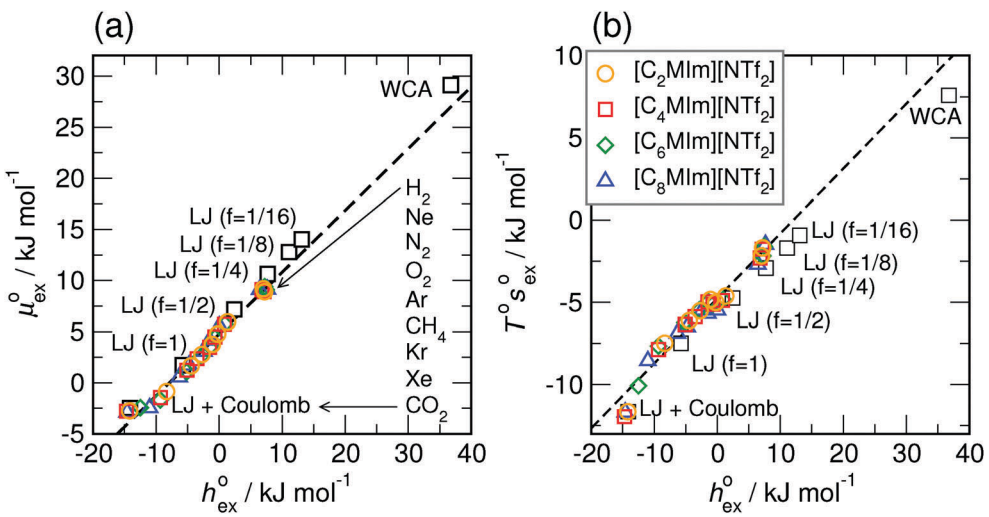

Fig. 4 (a) Correlation between the solvation free energy μ°_{ex} and the solvation enthalpy h°_{ex} of gases dissolved in [$C_n$mim][NTf_2] in the reference state. (b) Correlation between the solvation entropy s°_{ex} and the solvation enthalpy h°_{ex}. Shown are data for all other examined gases (colored) as well as the scaled potential model variants of CO_2 (black squares), taken from ref. 59.

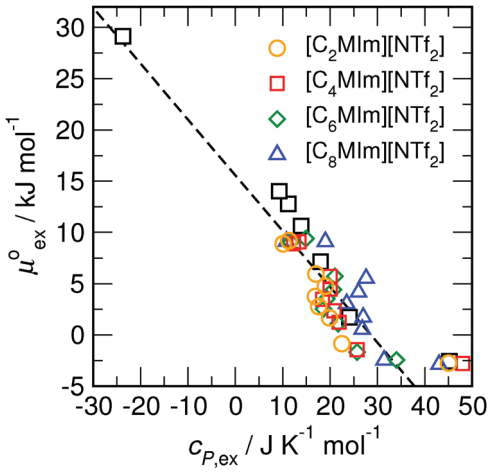

Fig. 5 Correlation between the solvation free energy μ°_{ex} and the solvation heat capacity $c_{P,ex}$ dissolved in [C$_n$mim][NTf$_2$] obtained for the different potential model variants of CO_2 (black)[59] and for all other examined gases (colored) under standard conditions.

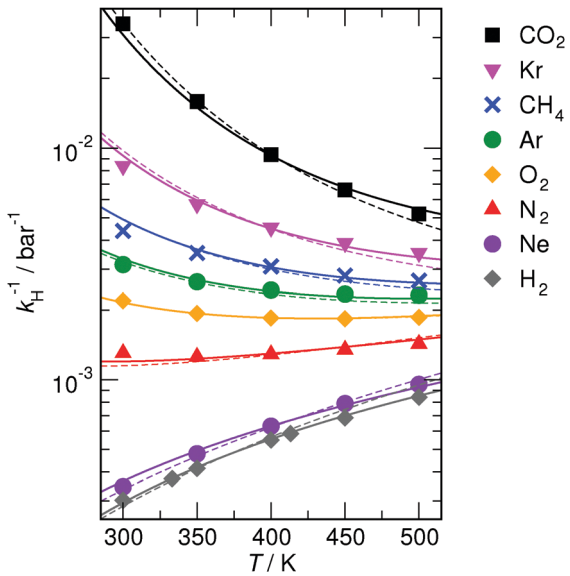

Fig. 6 The symbols denote the temperature dependence of the inverse Henry coefficients for all simulated gases dissolved in [C$_6$mim][NTf$_2$]. The lines indicate the predictions of the enthalpy–entropy compensation model. Thin dashed lines: $c_{P,ex}$ = 20 J K^{-1} mol^{-1}. Heavy solid lines: $c_{P,ex}$ according to eqn (11).

with $c = -1.837 \times 10^{-3}$ K^{-1} and d = 28.621 J mol^{-1} K^{-1}. With just four parameters, it is now possible to quantitatively predict the temperature dependence of the solubility of all studied gases in all four solvents. The only requirement is the knowledge of the solubility of a gas at the reference temperature T°. These model predictions with variable $c_{P,ex}$ are represented by thick solid lines in Fig. 6 for all the studied gases.

In addition to the temperature dependent experimental data, we have included predictions according to our enthalpy–entropy compensation model also in Fig. 2. The thick dashed lines in Fig. 2 represent data chosen to match our simulation data. The thin dashed lines are used to illustrate the temperature evolution of the model predictions in the vicinity of one particular solute. Here reference solubilities were chosen to be half and twice the size of the reference-solubility used for matching our MD simulation data. It is quite evident that particularly for N_2 and H_2, several experimental datasets are incompatible with our model predictions. However, the red dashed lines shown in Fig. 2 demonstrate that the experimental data obtained by the Maurer group in Kaiserslautern (the data obtained from the study by Kumełan *et al.* are represented by red symbols in Fig. 2a, b, d and f) for a variety of solutes are consistently in very good agreement with the predictions of the enthalpy–entropy compensation model. This includes even the controversial case of molecular hydrogen.

Finally, we would put another argument forward, that a positive slope for the temperature dependence of the hydrogen-solubility data is a very likely scenario. Following the arguments of Hayduk and Laudie,[102] which have been reviewed and extended by Beutier and Renon,[103] all Henry coefficients and hence all solubilities obtained for a certain solvent should meet at the critical point of that solvent, in our case the ILs. The solubility data shown in Fig. 6 clearly indicate a convergent behavior with increasing temperature. By extrapolating the enthalpy–entropy compensation model to very high temperatures, we find that this convergence even continues. In addition, Fig. 7 demonstrates that by assuming $c_{P,ex}$ to be constant, the model even predicts a single common intersection temperature T^* for the solubility of all gases. Eqn (6) and (9) imply that the common temperature T^* is defined by

$$T^* = T^{\circ} \cdot \frac{a}{a-1} \tag{12}$$

with the corresponding common solvation free energy of

$$\mu_{ex}(T^*) = \frac{b}{1-a} + \frac{c_{P,ex}T^{\circ}}{1-a}\left[a \cdot \ln\left(\frac{a}{a-1}\right) - 1\right]. \tag{13}$$

It is remarkable that eqn (12) just requires the knowledge of the parameter a, defined in eqn (9), as well as the chosen reference temperature T°. By using a = 1.653 and T° = 298 K, we compute a common temperature of T^* = 754 K for all gases used in this study. The solubility curves intersect at a value of $\mu_{ex}(T^*)$ = 7.166 kJ mol^{-1} for the case of $c_{P,ex}$ = 20 J K^{-1} mol^{-1} (indicated in Fig. 7). However, by allowing $c_{P,ex}$ to vary slightly for each gas, this constraint of a common temperature is violated. This does not necessarily mean that our model is inadequate, but rather that the temperature range of our study is too far away from the critical temperature. It is not unlikely that, by approaching the critical point, the solvation heat capacities $c_{P,ex}$ will eventually converge, while the solvated gases maintain their solvation enthalpy–entropy correlation. This would again restore the common temperature feature. Although the predicted solubility-data with variable $c_{P,ex}$ do not meet exactly at a particular temperature, they show a region of nearest approximation around 1100 K, which is far above the decomposition point of any of the ILs. We would like to point out, however, that this coincides nicely with results obtained from the study by Rebelo *et al.*[104]

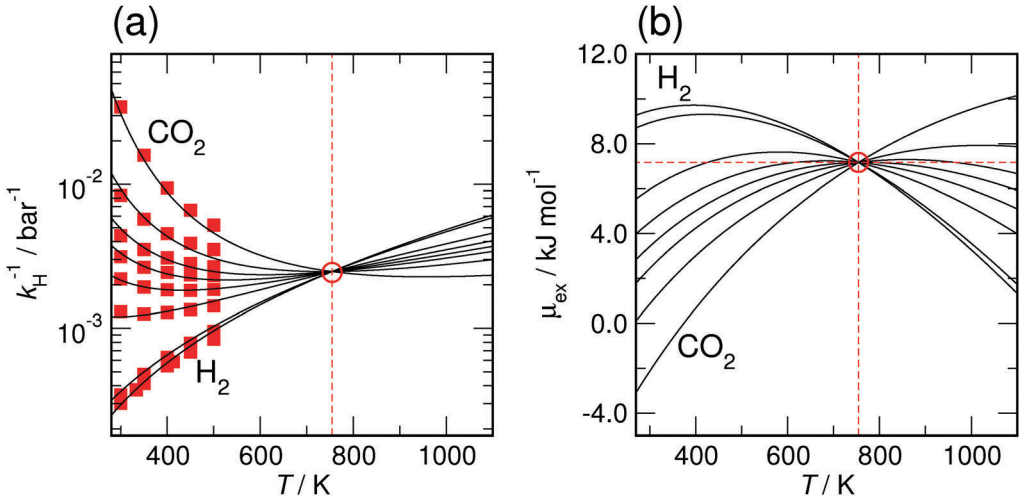

Fig. 7 Enthalpy–entropy compensation model predictions for all gases in [C_6mim][NTf_2] with a constant $c_{P,ex}$ = 20 J K^{-1} mol^{-1}. Indicated is the intersection temperature T^* = 754 K. (a) Predicted solubilities by inverse Henry coefficients. Red squares indicate the simulated values given in Table 2. (b) Predicted solvation free energies $\mu_{ex}(T)$.

and Freire *et al.*,[105] who estimated the location of the critical temperature to be around 1100 K using surface tension data in combination with the Eötvos and Guggenheim equations. The Monte Carlo simulations in the study by Rai *et al.*[106] as well as of Rane *et al.*[107] predict the critical temperatures of about 1200 K. These predicted critical temperatures, however, were significantly larger than the predictions of Yokozeki *et al.*,[108] who used the Vetere method, as well as of Shin *et al.*,[109] who used the group contribution method (GCM) of Joback, and Valderrama *et al.*,[110] who obtained results applying the modified Lydersen–Joback–Reid method (mLJR).

4 Conclusion

The systematic behavior of the gas solubility in ionic liquids is studied and described with the help of extensive molecular dynamics simulations. The solubility of hydrogen, oxygen, nitrogen, methane, krypton, argon, neon and carbon dioxide in the ionic liquids of type 1-*n*-alkyl-3-methylimidazolium bis(trifluoromethylsulfonyl)imide ([$C_n$mim][NTf_2]) with varying chain lengths n = 2, 4, 6, 8 is computed for a large temperature range from 300 K up to 500 K at 1 bar. By applying Widom's particle insertion technique, as well as Bennett's overlapping distribution method, we are able to determine solvation free energies of those selected light gases in imidazolium based ionic liquids with great statistical accuracy. A detailed comparison of the computed solubility data with available experimental and theoretical data is provided.

We observe that the chain length dependence of the computed solubility in various solvents can be mostly attributed to the change in the number-density of ion pairs in the solvent, as the computed solvation free energies show almost no chain length dependence.

The data obtained from our MD simulations clearly show that the magnitude of the solvation free energy at a defined reference temperature and its temperature-derivatives are intimately related to one another. This is a consequence of a solvation entropy–enthalpy compensation effect, which seems to be a defining feature of the solvation of small molecules in the investigated ionic liquids. This effect is leading to simple analytical relations quantitatively describing the temperature dependent solubility of gases solely depending on the absolute solubility value at a defined reference temperature.

The enthalpy–entropy compensation model is also predicts that the solubility data all meet at a single temperature, which is in line with the observation made for various fluids that the solubilities for gases meet at the critical temperature. However, this feature of a common temperature exists only, if the model is used with a unique heat capacity of solvation valid for all gases. Since the computed heat capacities of solvation do not vary strongly for different gases, a common value of $c_{P,ex}$ = 20 J K^{-1} mol^{-1} is a reasonable approximation for all the investigated solutes.

We would like to point out that the enthalpy–entropy compensation model is particularly helpful for assessing the solvation behavior of very light gases, such as hydrogen, where conflicting experimental data have been reported.

Acknowledgements

This work has been supported by the German Science Foundation (DFG) priority program SPP 1570 with additional support from SFB 652.

References

1 P. Wasserscheid and T. Welton, *Ionic Liquids in Synthesis*, VCH-Wiley, Weinheim, 2nd edn, 2007.
2 C. A. Angell, Y. Ansari and Z. Zhao, *Faraday Discuss.*, 2012, **154**, 9–27.

3 F. Endres and S. Z. El Abedin, *Phys. Chem. Chem. Phys.*, 2006, **8**, 2101–2116.
4 R. D. Rogers and K. R. Seddon, *Science*, 2003, **302**, 792–793.
5 M. Smiglak, A. Metlen and R. D. Rogers, *Acc. Chem. Res.*, 2007, **40**, 1182–1192.
6 N. V. Plechkova and K. R. Seddon, *Chem. Rev.*, 2008, **37**, 123–150.
7 L. A. Blanchard, D. Hancu, E. J. Beckman and J. F. Brennecke, *Nature*, 1999, **399**, 28–29.
8 D. J. Tempel, P. B. Henderson, J. R. Brzozowski, R. M. Pearlstein and H. Cheng, *J. Am. Chem. Soc.*, 2008, **130**, 400–401.
9 J. Huang and T. Rüther, *Aust. J. Chem.*, 2009, **62**, 298–308.
10 M. Ramdin, T. W. de Loos and T. J. H. Vlugt, *Ind. Eng. Chem. Res.*, 2012, **51**, 8149–8177.
11 J. E. Bara, D. E. Camper, D. L. Gin and R. D. Noble, *Acc. Chem. Res.*, 2010, **43**, 152–159.
12 S. Raeissi and C. J. Peters, *Green Chem.*, 2009, **11**, 185–192.
13 C. Myers, H. Pennline, D. Luebke, J. Ilconich, J. K. Dixon, E. J. Maginn and J. F. Brennecke, *J. Membr. Sci.*, 2008, **322**, 28–31.
14 J. Ilconich, C. Myers, H. Pennline and D. Luebke, *J. Membr. Sci.*, 2007, **298**, 41–47.
15 Z. Lei, C. Dai and B. Chen, *Chem. Rev.*, 2013, **114**, 1289–1326.
16 A. Finotello, J. E. Bara, D. Camper and R. D. Noble, *Ind. Eng. Chem. Res.*, 2008, **47**, 3453–3459.
17 J. Jacquemin, P. Husson, V. Majer and M. F. Costa Gomes, *J. Solution Chem.*, 2007, **36**, 967–979.
18 M. F. Costa Gomes, *J. Chem. Eng. Data*, 2007, **52**, 472–475.
19 J. Kumełan, A. P. S. Kamps, D. Tuma and G. Maurer, *J. Chem. Thermodyn.*, 2006, **38**, 1396–1401.
20 P. J. Dyson, G. Laurenczy, C. A. Ohlin, J. Vallance and T. Welton, *Chem. Commun.*, 2003, 2418–2419.
21 J. Jacquemin, M. F. Costa Gomes, P. Husson and V. Majer, *J. Chem. Thermodyn.*, 2006, **38**, 490–502.
22 J. Jacquemin, P. Husson, V. Majer, A. A. H. Padua and M. F. Costa Gomes, *Green Chem.*, 2008, **10**, 944–950.
23 J. Jacquemin, P. Husson, V. Majer and M. F. Costa Gomes, *Fluid Phase Equilib.*, 2006, **1**, 87–95.
24 J. Kumełan, A. P. S. Kamps, D. Tuma and G. Maurer, *J. Chem. Eng. Data*, 2006, **51**, 11–14.
25 J. Kumełan, D. Tuma, A. P. S. Kamps and G. Maurer, *J. Chem. Eng. Data*, 2010, **55**, 165–172.
26 S. Raeissi, L. J. Florusse and C. J. Peters, *J. Chem. Eng. Data*, 2011, **56**, 1105–1107.
27 Y. Shimoyama and A. Ito, *Fluid Phase Equilib.*, 2010, **297**, 178–182.
28 N. A. Manan, C. Hardacre, J. Jacquemin, D. W. Rooney and T. G. A. Youngs, *J. Chem. Eng. Data*, 2009, **54**, 2005–2022.
29 J. Palomar, M. Gonzalez-Miquel, A. Polo and F. Rodriguez, *Ind. Eng. Chem. Res.*, 2011, **50**, 3452–3463.
30 K. Z. Sumon and A. Henni, *Fluid Phase Equilib.*, 2011, **310**, 39–55.
31 J. Abildskov, M. D. Ellegaard and J. P. O'Connell, *Fluid Phase Equilib.*, 2009, **286**, 95–106.
32 J. S. Andreu and L. F. Vega, *J. Phys. Chem. B*, 2008, **112**, 15398–15406.
33 X. Zhang, Z. Liu and W. Wang, *AIChE J.*, 2008, **54**, 2717–2728.
34 J. S. Andreu and L. F. Vega, *J. Phys. Chem. C*, 2007, **111**, 16028–16034.
35 Y. S. Kim, J. H. Jang, B. D. Lim, J. W. Kang and C. S. Lee, *Fluid Phase Equilib.*, 2007, **256**, 70–74.
36 A. A. Oliferenko, P. V. Oliferenko, K. R. Seddon and J. S. Torrecilla, *Phys. Chem. Chem. Phys.*, 2011, **13**, 17262–17272.
37 E. J. Maginn, *J. Phys.: Condens. Matter*, 2009, **21**, 373101.
38 W. Shi and E. J. Maginn, *J. Phys. Chem. B*, 2008, **112**, 2045–2055.
39 W. Shi and E. J. Maginn, *J. Phys. Chem. B*, 2008, **112**, 16710–16720.
40 T. Köddermann, D. Paschek and R. Ludwig, *ChemPhysChem*, 2008, **9**, 549–555.
41 R. M. Lynden-Bell, N. A. Atamas, A. Vasilyuk and C. G. Hanke, *Mol. Phys.*, 2002, **100**, 3225–3229.
42 C. G. Hanke, A. Johansson, J. B. Harper and R. M. Lynden-Bell, *Chem. Phys. Lett.*, 2003, **374**, 85–89.
43 J. Deschamps, M. F. Costa Gomes and A. A. H. Padua, *ChemPhysChem*, 2004, **5**, 1049–1052.
44 J. K. Shah and E. J. Maginn, *Fluid Phase Equilib.*, 2004, **195**, 222–223.
45 J. K. Shah and E. J. Maginn, *J. Phys. Chem. B*, 2005, **109**, 10395–10405.
46 C. Cadena, J. L. Anthony, J. K. Shah, T. I. Morrow, J. F. Brennecke and E. J. Maginn, *J. Am. Chem. Soc.*, 2004, **126**, 5300–5308.
47 J. Kumełan, A. P. S. Kamps, I. Urukova, D. Tuma and G. Maurer, *J. Chem. Thermodyn.*, 2005, **37**, 595–602.
48 I. Urukova, J. Vorholz and G. Maurer, *J. Phys. Chem. B*, 2005, **109**, 12154–12159.
49 J. Kumełan, A. P. S. Kamps, D. Tuma and G. Maurer, *Ind. Eng. Chem. Res.*, 2007, **46**, 8236–8240.
50 J. Deschamps and A. A. H. Pádua, *ACS Symp. Ser.*, 2005, **901**, 150–158.
51 X. P. Wu, Z. P. Liu and W. C. Wang, *Wuli Huaxue Xuebao*, 2005, **21**, 1138–1142.
52 W. Shi, D. C. Sorescu, D. R. Luebke, M. J. Keller and S. Wickramanayake, *J. Phys. Chem. B*, 2010, **114**, 6531–6541.
53 A. F. Ghobadi, V. Taghikhani and J. R. Elliott, *J. Phys. Chem. B*, 2011, **115**, 13599–13607.
54 R. Singh, E. Marin-Rimoldi and E. J. Maginn, *Ind. Eng. Chem. Res.*, 2015, **54**, 4385–4395.
55 F. Dommert, K. Wendler, R. Berger, L. Delle Site and C. Holm, *ChemPhysChem*, 2012, **13**, 1625–1637.
56 J. N. Canongia Lopes, J. Deschamps and A. A. H. Padua, *J. Phys. Chem. B*, 2004, **108**, 2038–2047.
57 T. Köddermann, D. Paschek and R. Ludwig, *ChemPhysChem*, 2007, **8**, 2464–2470.
58 D. Paschek, T. Köddermann and R. Ludwig, *Phys. Rev. Lett.*, 2008, **100**, 115901.
59 D. Kerlé, R. Ludwig, A. Geiger and D. Paschek, *J. Phys. Chem. B*, 2009, **113**, 12727–12735.
60 L. R. Pratt, *Annu. Rev. Phys. Chem.*, 2003, **53**, 409–436.

61 N. T. Southall, K. A. Dill and A. D. J. Haymet, *J. Phys. Chem. B*, 2002, **106**, 521–533.
62 B. Widom, P. Bhimalapuram and K. Koga, *Phys. Chem. Chem. Phys.*, 2003, **5**, 3085–3093.
63 D. Chandler, *Nature*, 2005, **437**, 640–647.
64 B. Wittich and U. K. Deiters, *J. Phys. Chem. B*, 2010, **114**, 3452–3463.
65 K. Patkowski, W. Cencek, P. Jankowski, K. Szalewicz, J. Mehl, G. Garberoglio and A. H. Harvey, *J. Chem. Phys.*, 2008, **129**, 094304.
66 B. Guillot and Y. Guissani, *J. Chem. Phys.*, 1993, **99**, 8075–8094.
67 J. Potoff and J. I. Siepmann, *AIChE J.*, 2001, **47**, 1676–1682.
68 N. Hansen, F. A. B. Agbor and F. J. Keil, *Fluid Phase Equilib.*, 2007, **259**, 180–188.
69 J. G. Harris and K. H. Yung, *J. Phys. Chem.*, 1995, **99**, 12021–12024.
70 E. Lindahl, B. Hess and D. van der Spoel, *J. Mol. Model.*, 2001, **7**, 306–317.
71 D. Paschek, *MOSCITO 4: MD simulation package*, 2008, http://ganter.chemie.uni-dortmund.de/MOSCITO.
72 S. Nosé, *Mol. Phys.*, 1984, **52**, 255–268.
73 W. G. Hoover, *Phys. Rev. A: At., Mol., Opt. Phys.*, 1985, **31**, 1695–1697.
74 M. Parrinello and A. Rahman, *J. Appl. Phys.*, 1981, **52**, 7182–7190.
75 S. Nosé and M. L. Klein, *Mol. Phys.*, 1983, **50**, 1055–1076.
76 U. Essmann, L. Perera, M. L. Berkowitz, T. A. Darden, H. Lee and L. G. Pedersen, *J. Chem. Phys.*, 1995, **103**, 8577–8593.
77 J. P. Ryckaert, G. Ciccotti and H. J. C. Berendsen, *J. Comput. Phys.*, 1977, **23**, 327–341.
78 R. P. Kennan and G. L. Pollack, *J. Chem. Phys.*, 1990, **93**, 2724–2735.
79 B. Widom, *J. Chem. Phys.*, 1963, **39**, 2808–2812.
80 T. L. Beck, M. E. Paulaitis and L. R. Pratt, *The Potential Distribution Theorem and Models of Molecular Solutions*, Cambridge University Press, Cambrigde, UK, 2006.
81 C. H. Bennett, *J. Comput. Phys.*, 1976, **22**, 245–268.
82 K. S. Shing and K. E. Gubbins, *Mol. Phys.*, 1983, **49**, 1121–1138.
83 D. Frenkel and B. Smit, *Understanding Molecular Simulation. From Algorithms to Applications*, Academic Press, San Diego, 2nd edn, 2002.
84 D. Paschek, *J. Chem. Phys.*, 2004, **120**, 6674–6690.
85 J. E. Roberts and J. Schnitker, *J. Chem. Phys.*, 1994, **101**, 5024–5031.
86 D. Paschek, *J. Chem. Phys.*, 2004, **120**, 10605–10617.
87 To interconvert solvation free energies μ_{ex} and Henry constants k_H, we use a second order polynomial fitted to the temperature dependent ion-pair density of the simulated ILs: $\rho_{IL}(T) = \rho_{IL}^{(0)} + \rho_{IL}^{(1)}\cdot T + \rho_{IL}^{(2)}\cdot T^2$. [$C_2$mim][$NTf_2$]: $\rho_{IL}^{(0)} = 2.985\ nm^{-3}$, $\rho_{IL}^{(1)} = -2.51 \times 10^{-3}\ nm^{-3}\ K^{-1}$, and $\rho_{IL}^{(2)} = 8.46 \times 10^{-7}\ nm^{-3}\ K^{-2}$. [$C_4$mim][$NTf_2$]: $\rho_{IL}^{(0)} = 2.639\ nm^{-3}$, $\rho_{IL}^{(1)} = -2.18 \times 10^{-3}\ nm^{-3}\ K^{-1}$, and $\rho_{IL}^{(2)} = 6.85 \times 10^{-7}\ nm^{-3}\ K^{-2}$. [$C_6$mim][$NTf_2$]: $\rho_{IL}^{(0)} = 2.368\ nm^{-3}$, $\rho_{IL}^{(1)} = -1.94 \times 10^{-3}\ nm^{-3}\ K^{-1}$, and $\rho_{IL}^{(2)} = 5.90 \times 10^{-7}\ nm^{-3}\ K^{-2}$. [$C_8$mim][$NTf_2$]: $\rho_{IL}^{(0)} = 2.127\ nm^{-3}$, $\rho_{IL}^{(1)} = -1.56 \times 10^{-3}\ nm^{-3}\ K^{-1}$, and $\rho_{IL}^{(2)} = 2.92 \times 10^{-7}\ nm^{-3}\ K^{-2}$.
88 K. N. Marsh, J. F. Brennecke, R. D. Chirico, M. Frenkel, A. Heintz, J. W. Magee, C. J. Peters, L. P. N. Rebelo and K. R. Seddon, *Pure Appl. Chem.*, 2009, **81**, 781–790.
89 R. D. Chirico, V. Diky, J. W. Magee, M. Frenkel and K. N. Marsh, *Pure Appl. Chem.*, 2009, **81**, 791–828.
90 J. Kumełan, A. P. S. Kamps, D. Tuma and G. Maurer, *J. Chem. Thermodyn.*, 2006, **38**, 1396–1401.
91 S. S. Moganty and R. E. Baltus, *Ind. Eng. Chem. Res.*, 2010, **49**, 5846–5853.
92 D. Kerlé, R. Ludwig, A. Geiger and D. Paschek, *Z. Phys. Chem.*, 2013, **227**, 167–176.
93 D. Camper, J. Bara, C. Koval and R. Noble, *Ind. Eng. Chem. Res.*, 2006, **45**, 6279–6283.
94 J. L. Anderson, J. K. Dixon and J. F. Brennecke, *Acc. Chem. Res.*, 2007, **40**, 1208–1216.
95 J. Blath, M. Christ, N. Deubler, T. Hirth and T. Schiestel, *Chem. Eng. J.*, 2011, **172**, 167–176.
96 W. Afzal, X. Liu and J. M. Prausnitz, *J. Chem. Thermodyn.*, 2013, **63**, 88–94.
97 J. Kumełan, A. P. S. Kamps, D. Tuma and G. Maurer, *J. Chem. Eng. Data*, 2009, **54**, 966–971.
98 J. L. Anthony, J. L. Anderson, E. J. Maginn and J. F. Brennecke, *J. Phys. Chem. B*, 2005, **109**, 6366–6374.
99 J. Kumełan, A. P. S. Kamps, D. Tuma and G. Maurer, *J. Chem. Eng. Data*, 2006, **51**, 1364–1367.
100 R. Simha and T. Somcynsky, *Macromolecules*, 1969, **2**, 342–350.
101 H. Xie and R. Simha, *Polym. Int.*, 1997, **44**, 348–355.
102 W. Hayduk and H. Laudie, *AIChE J.*, 1973, **19**, 1233–1238.
103 D. Beutier and H. Renon, *AIChE J.*, 1978, **24**, 1122–1125.
104 L. P. N. Rebelo, J. N. Canongia Lopes, J. M. S. S. Esperança and E. Filipe, *J. Phys. Chem. B*, 2005, **109**, 6040–6043.
105 M. G. Freire, P. J. Carvalho, A. M. Fernandes, I. M. Marrucho, A. J. Queimada and J. A. P. Coutinho, *J. Colloid Interface Sci.*, 2007, **314**, 621–630.
106 N. Rai and E. J. Maginn, *Faraday Discuss.*, 2012, **154**, 53–69.
107 K. S. Rane and J. R. Errington, *J. Phys. Chem. B*, 2014, **118**, 8734–8743.
108 A. Yokozeki, M. B. Shiflett, C. P. Junk, L. M. Grieco and T. Foo, *J. Phys. Chem. B*, 2008, **112**, 16654–16663.
109 E.-K. Shin, B.-C. Lee and J. S. Lim, *J. Supercrit. Fluids*, 2008, **45**, 282–292.
110 J. O. Valderrama and P. A. Robles, *Ind. Eng. Chem. Res.*, 2007, **46**, 1338–1344.